Postprint of: Wójcik N., Polcyn K., Karczewski J., Górnicka K., Barczyński R., High-conducting $Bi_4V_{2-x}Fe_xO_{11-\delta}$ ceramics containing Fe_2O_3 nanocrystals: Structure and properties, JOURNAL OF THE EUROPEAN CERAMIC SOCIETY (2022), DOI: 10.1016/j.jeurceramsoc.2022.05.012

© 2022. This manuscript version is made available under the CC-BY-NC-ND 4.0 license https://creativecommons.org/licenses/by-nc-nd/4.0/

Journal Pre-proof

High-conducting $Bi_4V_{2-x}Fe_xO_{11-\delta}$ ceramics containing Fe_2O_3 nanocrystals: Structure and properties

N.A. Wójcik, K. Polcyn, J. Karczewski, K. Górnicka, R.J. Barczyński

PII: S0955-2219(22)00356-9

DOI: https://doi.org/10.1016/j.jeurceramsoc.2022.05.012

Reference: JECS14843

To appear in: *Journal of the European Ceramic Society*

Received date: 1 March 2022
Revised date: 28 April 2022
Accepted date: 6 May 2022

Please cite this article as: N.A. Wójcik, K. Polcyn, J. Karczewski, K. Górnicka and R.J. Barczyński, High-conducting $Bi_4V_{2-x}Fe_xO_{11-\delta}$ ceramics containing Fe_2O_3 nanocrystals: Structure and properties, *Journal of the European Ceramic Society,* (2022) doi:https://doi.org/10.1016/j.jeurceramsoc.2022.05.012

This is a PDF file of an article that has undergone enhancements after acceptance, such as the addition of a cover page and metadata, and formatting for readability, but it is not yet the definitive version of record. This version will undergo additional copyediting, typesetting and review before it is published in its final form, but we are providing this version to give early visibility of the article. Please note that, during the production process, errors may be discovered which could affect the content, and all legal disclaimers that apply to the journal pertain.

© 2022 Published by Elsevier.

Journal Pre-proof

High-conducting $Bi_4V_{2-x}Fe_xO_{11-\delta}$ ceramics containing Fe_2O_3 nanocrystals: Structure and properties

N. A. Wójcik[1*], K. Polcyn[1], J. Karczewski[1], K. Górnicka[1], R. J. Barczyński[1]

[1] *Advanced Materials Center, Institute of Nanotechnology and Materials Engeenering, Gdańsk University of Technology, 11/12 G. Narutowicza Street, 80-233 Gdańsk, Poland*

**corresponding author:* natalia.wojcik@pg.edu.pl,

Keywords: $Bi_4V_{2-x}Fe_xO_{11-\delta}$, Fe_2O_3 nanocrystals, X-ray diffraction, Morin transition, Impedance spectroscopy

Abstract

The topography, structure, thermal, magnetic, and electrical properties of $Bi_4V_{2-x}Fe_xO_{11-\delta}$ ceramics substituted with x = 0.5 and 0.7 Fe were studied. The microscope analysis showed the presence of iron-rich nanocrystals formed on the Bi-Fe-V-O grains. The X-ray diffraction studies confirmed that grains are built mostly of tetragonal $Bi_4V_{1.5}Fe_{0.5}O_{10.5}$ phase. Thermal properties analysis showed an order-disorder type γ ↔ γ´ phase transition at a temperature of around 916 K, pronounced in samples doped with x = 0.5 Fe. The magnetic anomaly was observed in ceramics doped with x = 0.7 Fe which was assigned to Morin transition of Fe_2O_3. The conductivity was measured over a wide frequency range from 10 mHz to 1 MHz and at a wide temperature range from 373 to 923 K, using impedance spectroscopy. The D.C. conduction process was due to oxygen vacancies hopping while at low temperatures electron holes hopping is also possible.

1. Introduction

In recent years, there has been a great interest in a family of bismuth layered oxides so-called BIMEVOX because of their high anionic conductivity and their possible certain electronic applications [1–6] for example in solid oxide fuel cells [7], in small-scale ceramic oxygen generators for aeronautical or medical applications [8]. These compounds are derived from $Bi_4V_2O_{11}$ ceramic which exhibits ferroelectric properties at room temperature

Journal Pre-proof

MOST WIEDZY Downloaded from mostwiedzy.pl

[3,4,9]. Since the discovery of $Bi_2V_4O_{11}$, a lot of investigations have been conducted to stabilize, at room temperature, the highest conducting γ-tetragonal high-temperature phase [1,5,8,10]. Moreover, the $Bi_2V_4O_{11}$ ceramic can be found also as a noncentrosymmetric orthorhombic α-phase at room temperature and a centrosymmetric orthorhombic β-phase at temperatures between 730 K and 835 K. It melts at 1153 K. The high-temperature γ-phase observed above 835 K, consists of $(Bi_2O_2)^{2+}$ sheets interleaved with perovskite like layers of $(VO_{3.5}\square_{0.5})^{2-}$ where □ is an oxygen ion vacancies [9,11]. The presence of oxygen vacancies is a consequence of the occurred in ceramic, reduced valance state of vanadium ions (V^{4+}). Due to that, the formation of oxygen vacancy with two tetravalent vanadium ions is necessary to maintain the electrical neutrality of the crystal structure. Accordingly, the high anionic conductivity visible in γ-phase is caused by the presence of oxygen ion vacancies (with two effective positive charges) in the perovskite layer. Those vacancies are known to be the most mobile charge carriers in perovskite ferroelectrics [6,12].

The ion conduction process is thermally activated and is due to the hops of oxygen ion vacancies through the crystal lattice [13,14]. It is highly dependent on the crystal structure, defects, and disorder of oxygen vacancies. Therefore, the doping of $Bi_4V_2O_{11}$ with different metals can significantly influence the crystal structure and as follows the oxygen vacancies diffusion pathways. Especially, the most popular is the substitution of vanadium by iso- or aliovalent cations in the perovskite-like layer like Cu [8,15], Co [16], Cr [2], Cd [16], U [1], Ti [17], P [18], W [5], etc. Doping with cations of valence different than vanadium influences the symmetry and the connectivity of the polyhedra inside the perovskite-like layer and allows to modify of the anionic vacancy concentration in crystals. Additionally, the substitutions by lower valence cations can introduce electronic carriers which can take part in the total conductivity process at low temperatures [19–23].

Journal Pre-proof

MOST WIEDZY Downloaded from mostwiedzy.pl

An interesting effect was found for the x = 0.5 Fe substitution for V which has resulted in the development of a new crystal structure $Bi_4Fe_{0.5}V_{1.5}O_{10.5}$. This composition exhibits tetragonal crystal symmetry with the lattice parameters: *a, b = 3.921, and c = 15.571 Å* and corresponds to the upper limit of the γ-type solid solution [2]. The lattice parameters for α-phase of un-doped $Bi_4V_2O_{11}$ are: *a = 5.543, b = 5.615, and c = 15.321 Å* at room temperature [4]. The new phase $Bi_4Fe_{0.5}V_{1.5}O_{10.5}$ exhibits higher conductivity than the un-doped one at the low-temperature region. High ionic conductivity makes it a good candidate for an electrolyte in SOFC and a competitor for the most commonly used, stabilized ZrO_2, which required a very high operating temperature (~ 1000 °C). Moreover, BIFEVOX as electrolytes have also the ability to dynamically self-transform into electrode materials under polarization, so this membrane could be used without other electrode materials [24,25].

Nowadays, composite materials are intensively considered for alternative electrolytes in SOFC. Using composites can improve the properties required for electrolytes [24]. Therefore, materials based on BIMEVOX ceramics and their components can give an opportunity to improve the quality of electrolyte material [24,26,27]. In the present study, the full characterization of the topography, structure, thermal, magnetic, and electrical properties of $Bi_4V_{2-x}Fe_xO_{11-\delta}$ ceramics is done by exploiting the advances of modern-day characterization techniques. The substitution was done for x = 0.5 Fe to obtain $Bi_4Fe_{0.5}V_{1.5}O_{10.5}$ single-phase and for x = 0.7 to exceed the iron solubility threshold. The modification was done using Fe_2O_3 and nanopowder Fe_3O_4 oxides to observe the possible differences in the synthesized materials.

2. Materials and methods

2.1. *Synthesis*

Journal Pre-proof

MOST WIEDZY Downloaded from mostwiedzy.pl

Four $Bi_4V_{2-x}Fe_xO_{11-\delta}$ ceramics in which x = 0.5 and 0.7 of V are substituted with Fe were synthesized via a conventional solid-state reaction route. The exact compositions of prepared samples are listed in Table 1. The samples IDs suggest the content of incorporated Fe and compound used for substitution: Fe_2O_3 or Fe_3O_4. The stoichiometric mixture of initial powders of Bi_2O_3 (POCH pure), V_2O_5 (ACROS 99,6+%), and Fe_2O_3 (Alfa Aesar 99,9%) or Fe_3O_4 nanopowder (Alfa Aesar 97% 50 – 100 nm) were ball-milled in pure isopropyl alcohol for 6 h. The milling was performed in steps of 50 min with rest intervals of 10 min. The mixture was dried at 373 K for 24 h in air. Powders were mixed in an agate mortar and cold-pressed into pellets (12 mm in diameter and 2–3 mm in thickness) under a compacting pressure of 20 kNm^{-2}. The obtained pellets were sintered at 1103 K for 24 h with heating and cooling rates of 1.5 $Kmin^{-1}$. Next, they were once again powdered and mixed in an agate mortar and pressed into pellets. The second heating was analogous to the first one.

2.2. Characterization

The structure has been studied by powder X-ray diffraction (XRD). XRD data were collected on a Bruker D2 PHASER diffractometer with CuK_α radiation (I = 1.5406 Å) and LynxEye-XE detector. The measurements were carried out over a 2θ range of 5–90° with a step size of 0.013° and a step time of 52 seconds. The XRD measurements were conducted at room temperature on powdered samples. The possible errors of XRD results were minimalized by removing the background and are included in the thickness of curves lines.

The topography of ceramics was observed on the surface and fresh cross-sections. Firstly, it was checked with an Olympus LEXT OLS4000 Confocal Scanning Laser Microscope (CSLM). Color imaging was performed under white LED light and 3D images were obtained using a 405 nm laser and Photomultiplier Detector. The maximum used

Journal Pre-proof

MOST WIEDZY Downloaded from mostwiedzy.pl

optical magnification was 2160x. Next, it was observed using Scanning Electron Microscope (SEM), FEI Company Quanta FEG250. The compositions of ceramics were studied using Energy Dispersive X-ray Spectrometer (EDX GENESIS Apex Apollo X60 Spectrometer). The EDX measurements were done at minimum three different points on the surface of visible grains for each sample, in the places without visible nanocrystals. The obtained results were similar and the mean values were taken for the metals ratio estimations. All metals contents were shown with the accuracy ± 3%. Additionally the EDX measurements were done for at least three points focused on the different nanocrystals, independently for each sample. X-ray Photoelectron Spectroscopy (XPS) was employed for the surface physico-chemical examination of the studied samples. The high-resolution XPS analyses were performed using an Escalab 250Xi device (ThermoFisher Scientific, USA), equipped with a monochromatic AlKα source. The adventitious carbon C 1s peak at 284.6 eV was used for the X-axis calibration of the XPS spectra. The measurements were done for the powdered samples.

Thermal effects were tested with the use of differential scanning calorimetry (DSC) up to 1000 °C in flowing nitrogen with a Netzsch STA 449 F1 instrument at a heating rate of 20 $Kmin^{-1}$. Proteus software provided by NETZSCH was used for the estimation of thermal properties parameters with the precision of ± 2 %. As Fe_3O_4 nanopowder was used for the samples preparation the possible magnetic effect was also checked with the use of Quantum Design Physical Property Measurement System (PPMS) with a vibrating sample magnetometer function (VSM) and the AC Measurement System (ACMS). Data were collected between 1.90 and 300 K in various magnetic fields for powdered samples.

Impedance spectroscopy measurements were conducted in the frequency range from 10 mHz to 1 MHz and the temperature range from 373 K to 913 K, with an A.C. voltage of 1 V_{rms}, using the Novocontrol Concept 40 broadband dielectric spectrometer Alpha-A, equipped with ZG4 dielectric interface. The temperature step was 10 K, measurements

MOST WIEDZY Downloaded from mostwiedzy.pl

were done during heating and cooling, in the air atmosphere. The temperature was controlled with Novotherm HT 1600. One test lasts about 4 days. The measurements were conducted two or three times on the same sample and a different sample of the same composition, to check the repeatability of results. For the electrical measurements, gold electrodes were evaporated in a vacuum at the polished plane-parallel surfaces of circular samples.

3. Results and discussion

3.1. Topography and structure

Four $Bi_4V_{2-x}Fe_xO_{11-\delta}$ ceramics substituted with x = 0.5 and 0.7 Fe were synthesized with the use of Fe_2O_3 and Fe_3O_4. The theoretical compositions estimated based on chemical reactions are listed in Tab. 1. The samples IDs suggested the content of Fe x = 0.5 or 0.7, and oxide used for synthesis: Fe_2O_3 or Fe_3O_4. Used magnetite Fe_3O_4 is a mixture of FeO and Fe_2O_3 and it decomposes at quite a low temperature (~ 823 K is below the synthesis temperature 1103 K) therefore the final content of oxygen can be different in the synthesized ceramics. In materials doped with two different transition metal ions like V and Fe, and synthesized at high temperatures, the redox reactions between ions of both metals lead to reduction or oxidation of one type of metal ions into one valence state while the second one stays in two different valence states. The XPS measurements were done for all samples to obtain the information about total Bi, V and Fe contents (Table 1), and to verify the possible presence of iron and vanadium ions in different valence states. The oxygen content is usually overestimated for XPS measurements therefore the mean results are shown as Bi:V:Fe metals ratios for theoretical and measured compositions in Tab. 1. The results suggest comparably higher content of Bi and consequently slightly lower content of Fe than theoretical ones. However, the underestimation of Fe amount can be due to observed halo of signal. The XPS Fe 2p spectrum recorded for all samples

Journal Pre-proof

MOST WIEDZY Downloaded from mostwiedzy.pl

suggests that Fe ions occur only as Fe^{3+}. As an example, the XPS V 2p spectra recorded for samples $0.7Fe_2O_3$ and $0.7Fe_3O_4$ are shown in Fig. 1 a and b, respectively. Based on the deconvolution results, it is possible to estimate V^{4+} and V^{5+} relative contents in each studied sample as listed in Table 1 in terms of the ratio. It can be seen that vanadium is primarily present in the lower valence state and its normalized to total vanadium content varies between 71% and 81% in samples. Moreover, the XPS results confirm that bismuth is present only in oxide form as Bi_2O_3 in all samples.

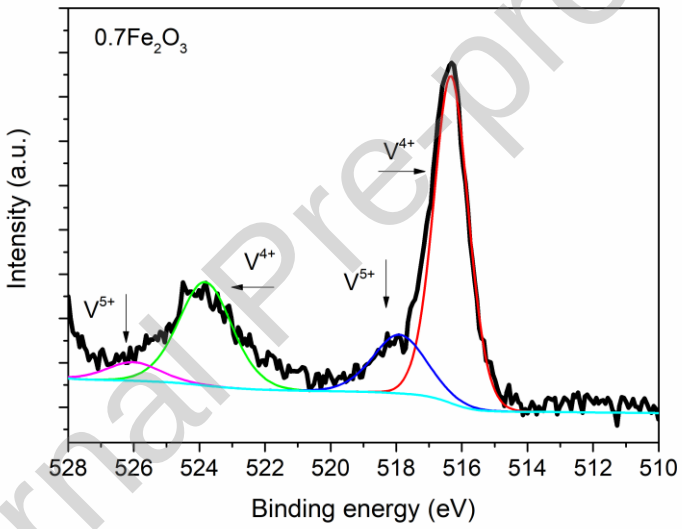

(a)

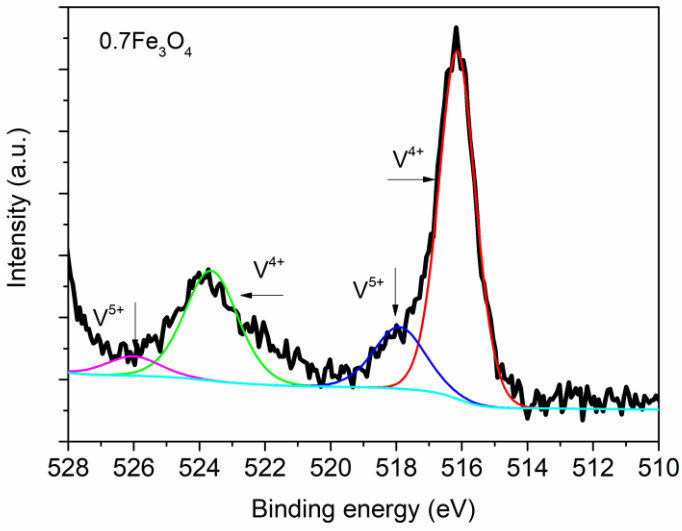

(b)

Figure 1. High-resolution XPS spectra recorded in a) V 2p core-level binding energy range for samples

Journal Pre-proof

MOST WIEDZY Downloaded from mostwiedzy.pl

(a) $0.7Fe_2O_3$ and (b) $0.7Fe_3O_4$.

Table 1. The compositions of samples estimated based on initial compositions, XPS results of powdered samples and EDX results at samples' surfaces.

Sample ID	Theoretical composition (at%)	Theoretical Bi:V:Fe ratio (at%)	Bi:V:Fe ratio estimated from XPS results ± 5% (at%)	V^{4+}/V^{5}+ ratio	$[V^{4+}]/([V^{4+}] + [V^{5+}])$ (%)	Bi:V:Fe ratio estimated from EDX for grains ± 3% (at%)
$0.5Fe_2O_3$	$Bi_4V_{1.5}Fe_{0.5}O_{10.5}$	67:25:8	70:25:4	4.2	81	68:20:12
$0.5Fe_3O_4$	$Bi_4V_{1.5}Fe_{0.5}O_{10.4}$	67:25:8	69:26:5	2.5	71	66:23:11
$0.7Fe_2O_3$	$Bi_4V_{1.3}Fe_{0.7}O_{10.3}$	67:22:12	71:24:5	3.7	78	68:20:12
$0.7Fe_3O_4$	$Bi_4V_{1.3}Fe_{0.7}O_{10.2}$	67:22:12	72:23:5	4.1	80	66:21:13

The surface topography of prepared ceramics was observed by the confocal microscopy technique. Figure 2 displays the obtained micrographs for samples: (left) 0.5 Fe_2O_3, (middle) 0.7 Fe_2O_3, and (right) 0.7 Fe_3O_4. The morphology of each ceramic contains grains of different shapes and sizes. Additionally, the grain boundaries and pores are visible in all materials. The mean size of grains was estimated with the use of dedicated software. The values obtained for samples vary between 4 μm and 21 μm. Additionally, the second phase of nanometer size is observed for all ceramics which is randomly distributed on the grains, and their content increases for samples doped with x = 0.7 Fe. In $0.7Fe_3O_4$ ceramic the content of the second phase is the highest.

Journal Pre-proof

MOST WIEDZY Downloaded from mostwiedzy.pl

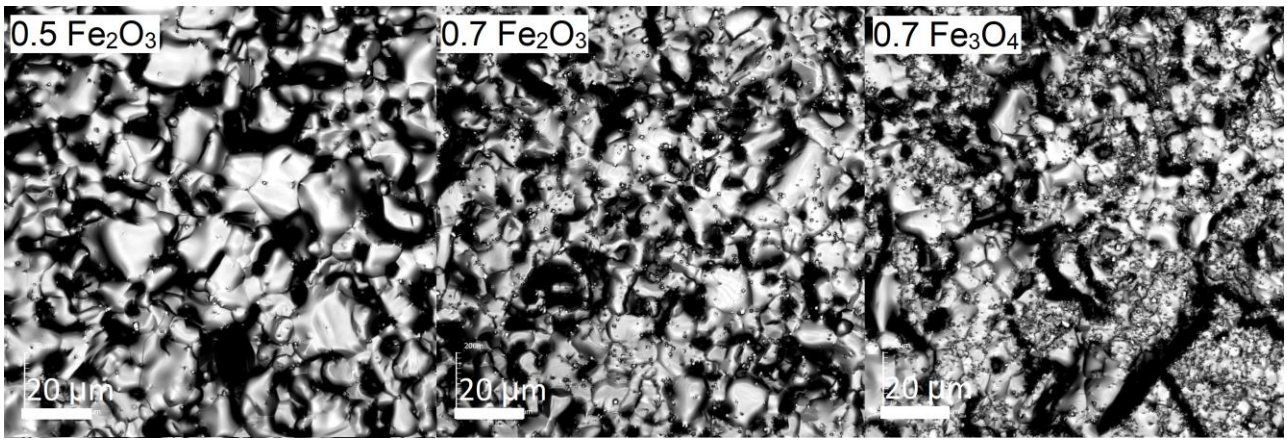

Figure 2. The topography of ceramics: (left) 0.5 Fe_2O_3, (middle) 0.7 Fe_2O_3, and (right) 0.7 Fe_3O_4 measured with Confocal microscope.

To estimate the mean size of the observed second phase, the SEM observations were done. Figure 3 presents the set of SEM micrographs for all samples. The topography of surfaces are shown for 0.5Fe_2O_3 sample in fig. 3 (left-up), 0.5 Fe_3O_4 (left-down), 0.7 Fe_2O_3 (right-up), and 0.7 Fe_3O_4 (right-down). The SEM observations are in accord with the Confocal microscope analysis. The second phase is also found in the pictures of cross-sections (not shown). Moreover, in bigger magnification, it is possible to observe that the shape of the second phase is cubical. Regular shape indicates their crystalline nature while their size varies between 70 nm and 700 nm. The highest number of nanocrystals is visible on the surface of the 0.7Fe_3O_4 sample.

Journal Pre-proof

MOST WIEDZY Downloaded from mostwiedzy.pl

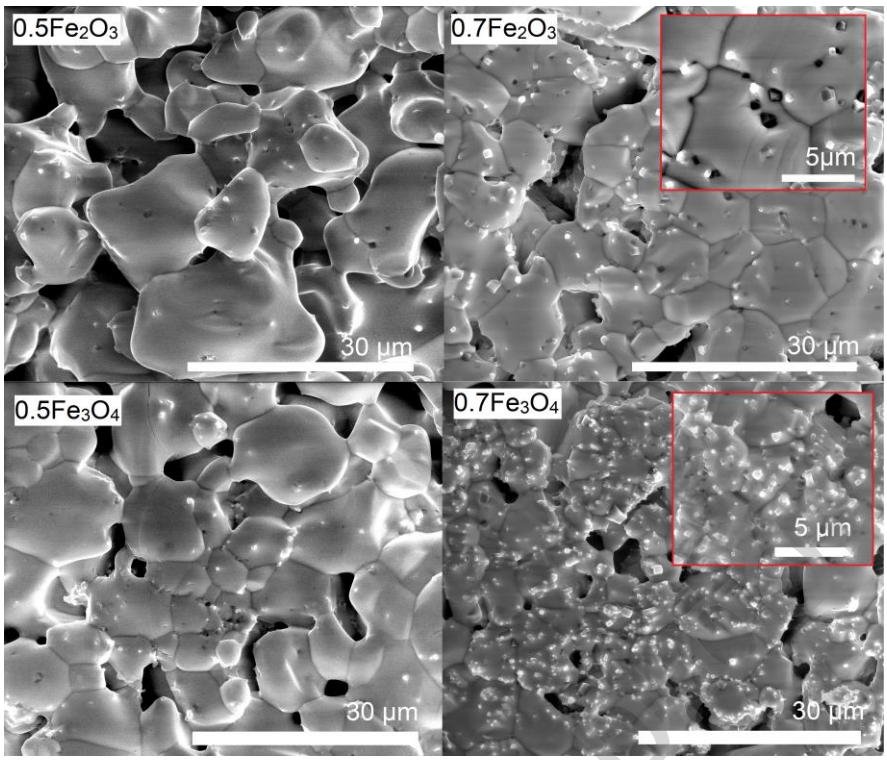

Figure 3. SEM micrographs for surfaces of: (left-up) 0.5 Fe_2O_3, (left-down) 0.5 Fe_3O_4, (right-up) 0.7 Fe_2O_3, and (right-down) 0.7 Fe_3O_4 samples.

The EDX measurements were done for both grains and nanocrystals. The oxygen content is usually overestimated for EDX measurements therefore the mean results for grains are shown as Bi:V:Fe metals ratios for measured compositions in Tab. 1. The Bi:V:Fe ratios obtained for grains for x = 0.7 Fe ceramics are in good agreement with the theoretical ones. In the case of x = 0.5 Fe ceramics, the results suggest comparably higher content of Fe and consequently slightly lower content of V. On the other hand, the nanocrystals are dominated by Fe. Probably, the visible nanocrystals are made of crystalline iron oxide. However, the size of visible structures is too low to confirm their exact compositions by EDX measurements, which showed also the results of grains.

Journal Pre-proof

MOST WIEDZY Downloaded from mostwiedzy.pl

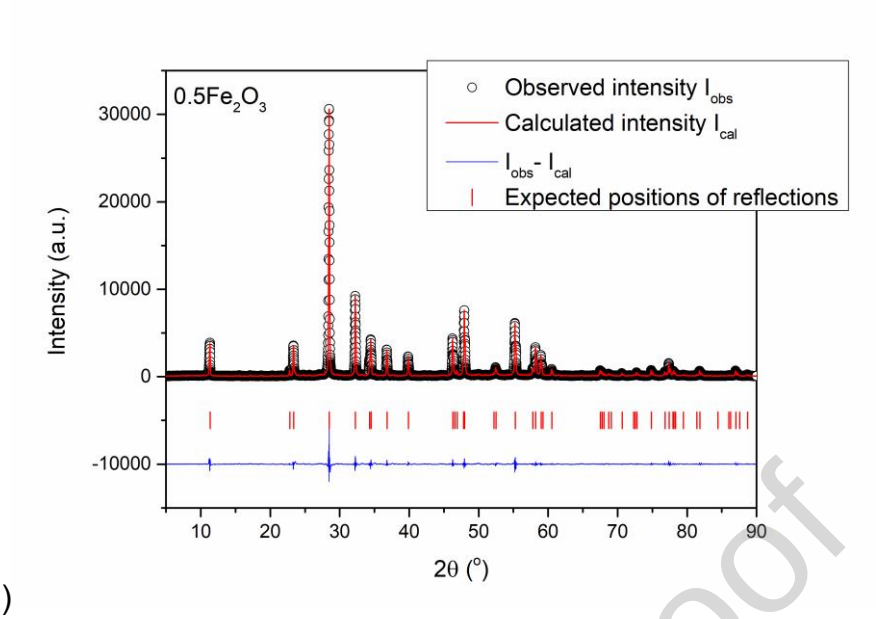

(a)

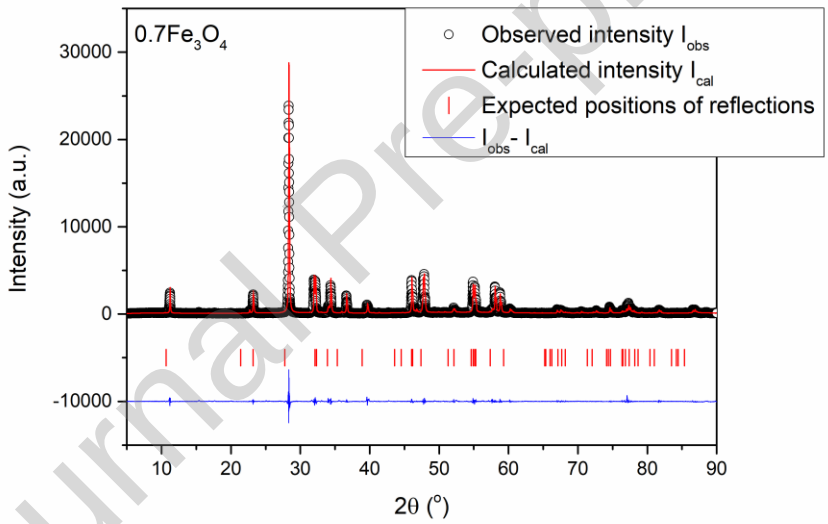

(b)

Figure 4. Powder X-ray diffraction pattern of **(a)** $0.5Fe_2O_3$ and **(b)** $0.7Fe_3O_4$ samples (black circles) together with the LeBail refinement profile (red solid line). The red vertical bars indicate the expected Bragg peak positions. The blue curve is the difference between experimental and model results.

Table 2. The lattice constants of the dominating $Bi_4V_{1.5}Fe_{0.5}O_{10.5}$ phase obtained from LeBail fit of the powder diffraction pattern results with unit cell scheme and the estimated distance between vanadium ions.

Tetragonal phase $Bi_4V_{1.5}Fe_{0.5}O_{10.5}$	$0.5Fe_2O_3$	$0.5Fe_3O_4$	$0.7Fe_2O_3$	$0.7Fe_3O_4$
(I4/mmm)				
Space group (139)				

Journal Pre-proof

MOST WIEDZY Downloaded from mostwiedzy.pl

lattice constants	a = 3.9200(4) Å c = 15.581(2) Å	a = 3.9204(3) Å c = 15.583(2) Å	a = 3.9278(4) Å c = 15.584(2) Å	a = 3.9284(7) Å c = 15.583(3) Å
V-V bond length	L_1 = 3.920 Å L_2 = 8.109 Å	L_1 = 3.920 Å L_2 = 8.110 Å	L_1 = 3.928 Å L_2 = 8.112 Å	L_1 = 3.928 Å L_2 = 8.111 Å
lattice constants			a = 3.940(2) Å c = 16.603(3) Å	a = 3.941(1) Å c = 16.606(3) Å
V-V bond length			L_1 = 3.940 Å L_2 = 8.604 Å	L_1 = 3.941 Å L_2 = 8.606 Å

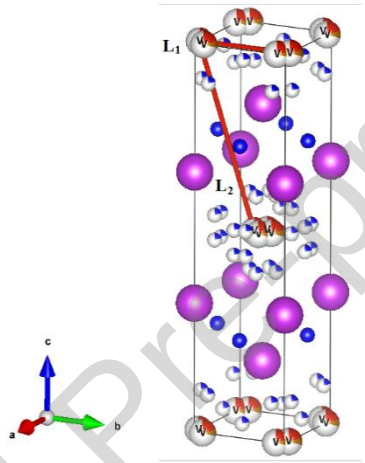

The X-ray diffractograms for exemplar ceramics are shown in figure 4. The pXRD confirmed a single-phase of $0.5Fe_2O_3$ and $0.5Fe_3O_4$ ceramics. In a more detailed analysis of the data, the tetragonal $Bi_4V_{1.5}Fe_{0.5}O_{10.5}$ (I4/mmm) phase was refined with the LeBail method. The results of LeBail fit to the powder diffraction pattern is represented by the black solid line in Fig. 4 for ceramics $0.5Fe_2O_3$ and $0.7Fe_3O_4$. The fit results obtained for the x = 0.5 Fe samples were analogous and gave the lattice constants a = 3.9200(4) Å and c = 15.581(2) Å (see Tab. 2). These values are in very good agreement with the data published previously [2]. The Bragg positions and the difference plot between experimental and fitted data (blue line) are also shown in Fig. 4. Ceramics doped with x = 0.7 Fe turned out to be two-phase. The dominating tetragonal $Bi_4V_{1.5}Fe_{0.5}O_{10.5}$ (I4/mmm) phase shown the lattice constants: a = 3.9279(8) Å and c = 15.584(3) Å, however fitting of few small reflections gave also slightly different lattice constants: a = 3.940(2) Å and c = 16.603(3) Å

Journal Pre-proof

MOST WIEDZY Downloaded from mostwiedzy.pl

(listed in Tab. 2). Additionally, small participation of orthorhombic $Bi_4Fe_{0.1}V_{1.9}O_{10.9}$ (Cmcm) phase with lattice constants: a = 15.475(7) Å, b = 5.584(1) Å and c = 10.979(3) Å, were found. The possible reflections corresponding to crystalline Fe_2O_3 are in the background-size intensity therefore, the occurrence of Fe_2O_3 nanocrystals cannot be confirmed by XRD.

The XRD results can give information about the mean crystallites size of which particles (grains) are built. The mean crystallites size of dominating phase was about 130 ± 10 nm in all ceramics, obtained from LeBail fit. The grains are often agglomerations of many crystallites therefore the mean grain size estimated from analysis of confocal microscope images is much higher. Additionally, the XRD data was used to estimate the distance between vanadium ions in the unit cell of dominating $Bi_4V_{1.5}Fe_{0.5}O_{10.5}$ phase. There are two possible vanadium ions‘ positions in tetragonal $Bi_4V_{1.5}Fe_{0.5}O_{10.5}$ (I4/mmm) phase: in the corners of the unit cell and in the middle of unit cell. In the first position the bond length between vanadium ions (L_1) is shorter and is directly correlated with the lattice constant a. In the second position, the V-V bond length, L_2 is more than two times longer than L_1. The estimated results of V-V bond length in both positions with unit cell scheme are presented in Table 2. It can be seen that the distances between vanadium ions (L_1 and L_2) are longer in the unit cell of ceramics doped with x = 0.7 Fe. Moreover, in these samples the V-V bond lenghts were estimated also for the second lattice constants of the same $Bi_4V_{1.5}Fe_{0.5}O_{10.5}$ phase. The obtained results were also higher than in ceramics doped with 0.5 Fe.

3.2. Thermal and magnetic properties

Un-doped $Bi_4V_2O_{11}$ ceramic exhibits two strong endothermic peaks, revealing the existence of the α↔β and β↔γ phase transitions, at temperatures 715 K and 840 K, respectively. The α↔β phase transition is the para-ferroelectric phase transition and determines the occurrence of ferroelectric properties in $Bi_4V_2O_{11}$ [6]. It was found that the

MOST WIEDZY Downloaded from mostwiedzy.pl

substitution of V with Fe up to x = 0.2 shifted the temperatures of phase transitions into lower temperatures with the increase in Fe content [2]. However, in the tested samples, the grains are built of the $Bi_4V_{1.5}Fe_{0.5}O_{10.5}$ phase which is a γ-phase and has already a tetragonal symmetry. For this, single-phase ceramic, no thermal effects were observed up to 873 K [2] while at a temperature of 890 K an order-disorder type γ ↔ γ´ phase transition was found (during heating in air atmosphere) [24].

The DSC curves for all synthesized ceramics are shown in figure 5. It can be seen that in the samples doped with x = 0.5 Fe the weak endothermic peak is visible around the temperature of 916 K. This effect was repetitive for the second measurement at the same sample. A similar effect is smoothed in the samples doped with x = 0.7 Fe. Most probably, the origin of the visible endothermic process is due to an order-disorder type γ ↔ γ´ phase transition [24]. The shift into higher temperatures can be due to different measurement techniques and parameters as well as the presence of nanocrystals on the grain surfaces.

The melting point for Fe-doped ceramics was estimated to be around 1193 K [3] which is slightly higher than the one for un-doped $Bi_4V_2O_{11}$, 1153 K.

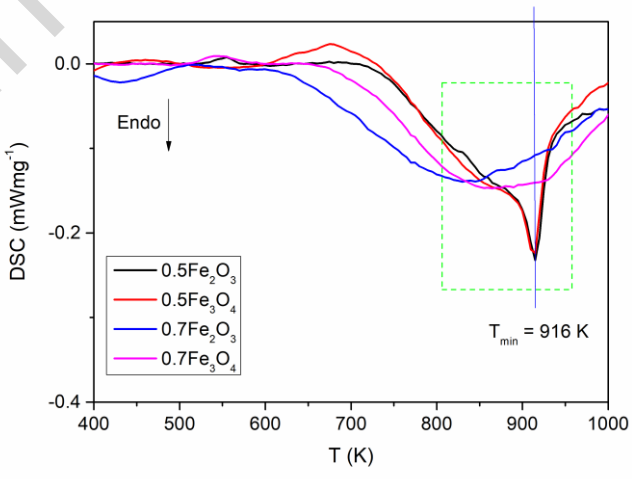

Figure 5. DSC curves for all samples.

Magnetic properties of ceramics were checked with the use of PPMS. All samples were found to be paramagnetic at low-temperature region and no hysteresis loop was observed.

Journal Pre-proof

MOST WIEDZY Downloaded from mostwiedzy.pl

Figure 6 presents the magnetization of ceramics doped with x = 0.7 Fe as a function of temperature in the range 200–300 K under an applied magnetic field of 1000 Oe. The very subtle high-temperature anomaly is assigned to crystalline Fe_2O_3 in which a Morin transition takes place. This magnetic phase transition (or spin-flop transition) in hematite is observed at ~250 K [28]. Below this temperature, the structure of hematite is antiferromagnetic and it changes to weakly ferromagnetic on heating through 250 K [21,28]. The Morin transition is more pronounced for the sample doped with Fe_2O_3 than for the one doped with Fe_3O_4. However, the analysis of confocal microscope images suggests that the content of iron oxide nanocrystals is higher for the $0.7Fe_3O_4$ sample than for $0.7Fe_2O_3$. The subtlety of visible anomaly does not allow to compare the content of Fe_2O_3 crystals in materials. A similar Morin transition effect was not detected for samples doped with x = 0.5 Fe suggesting too low content of Fe_2O_3 crystals.

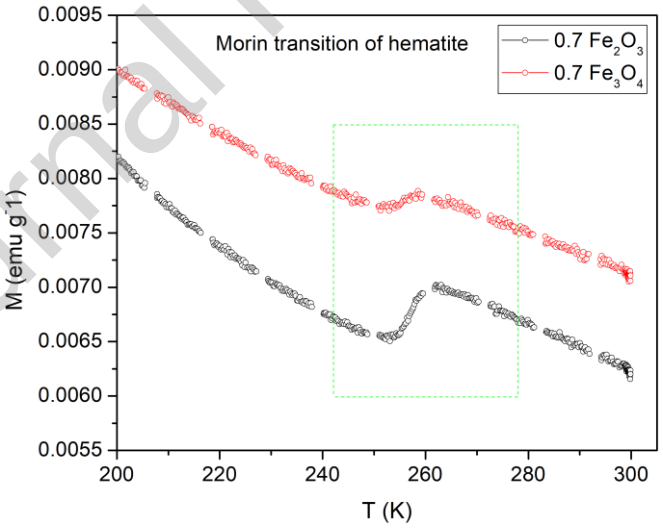

Figure 6. Dependence of magnetization on temperature under an applied magnetic field of 1000 Oe for $0.7Fe_2O_3$ and $0.7Fe_3O_4$ samples.

3.3. Electrical properties

The A.C. complex conductivity and electric permittivity were studied as the function of frequency and temperature. All measurements were done twice for heating and cooling

Journal Pre-proof

MOST WIEDZY Downloaded from mostwiedzy.pl

and results were found to be repetitive. The data obtained during heating overlap with the ones for cooling. The temperature hysteresis loop typical for ferroelectric $Bi_4V_2O_{11}$ [6] was not observed. Therefore, in this paper, we showed results only for the cooling process to facilitate the presentation. Figure 7 (a) presents the real part of electrical permittivity versus temperature measured at a frequency of 1 Hz, for all samples. The Reε increases with the temperature for all ceramics. For the samples with the same contents of iron, the results mostly overlap. The values found for x = 0.5 Fe ceramics are higher than for x = 0.7 Fe ceramics. Especially between 500 and 700 K, the difference is the highest, of more than one order of magnitude. However, there is no characteristic sharp increase in Reε around 700 K, found for ferroelectric $Bi_4V_2O_{11}$ [6]. The inset in figure 6(a) shows the electric permittivity behavior for different frequencies for the exemplar $0.5Fe_3O_4$ sample. The electric permittivity decrease with the increase in frequency. Results showed that the total polarization is higher in samples doped with lower Fe content. The polarization process can be influenced by the grain size, grain boundaries, defects, ionic conductivity, and other factors [12]. Therefore the structural changes that occurred in samples after doping with Fe may influence the polarization and consequently electric permittivity. It may be assumed that the increase in the nucleation of Fe_2O_3 nanocrystals, causes the decrease in electric permittivity in studied samples. At the same time samples doped with x = 0.5 Fe showed higher conductivity than samples with x = 0.7 Fe, as shown in Figure 7 (b). The higher conductivity at the high-temperature region can be due to the higher ionic conductivity of oxygen vacancies. The ion accumulation on grain boundaries can also increase the polarization effects [6,30].

Journal Pre-proof

MOST WIEDZY Downloaded from mostwiedzy.pl

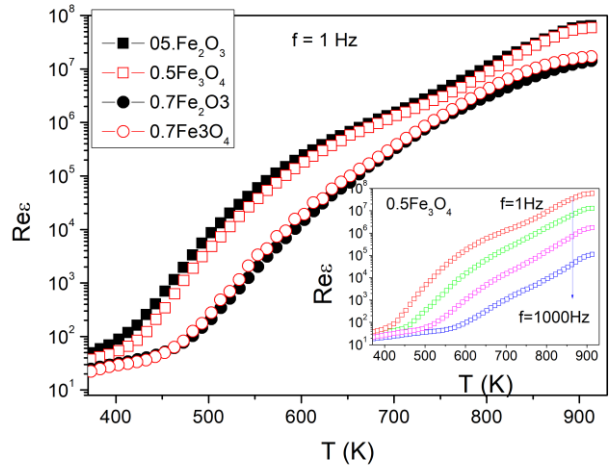

(a)

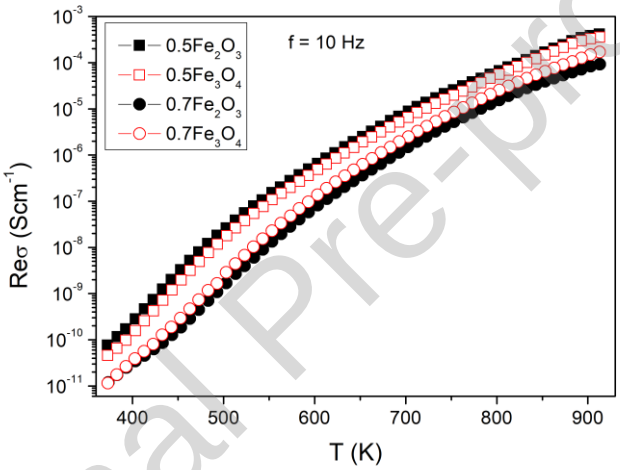

(b)

Figure 7. (a) The real part of electric permittivity and (b) the real part of A.C. conductivity as a function of temperature for all samples. Inset shows the Reε behavior for different frequencies.

The frequency dependences for A.C. conductivity are displayed in Figure 8 (a) and (b) for exemplar ceramics: $0.5Fe_2O_3$ and $0.7Fe_3O_4$, respectively. The conductivity spectra can be divided into two parts: low-frequency D.C. conductivity and high-frequency A.C. conductivity. The first part is visible as a frequency-independent plateau which for the temperature of 373 K reaches 3 decades of frequency and starts to dominate above 413 K in all samples. The second part increases with the frequency. The D.C. conductivity values were estimated from figure 8 and are presented in figure 8 versus reciprocal temperature. It may be seen that the D.C. conductivity is similar for samples doped with x = 0.5 Fe regardless of the dopant oxide. The D.C. conductivity decrease for ceramic $0.7Fe_3O_4$ and

Journal Pre-proof

MOST WIEDZY Downloaded from mostwiedzy.pl

is the lowest for ceramic $0.7Fe_2O_3$. Especially the biggest difference of two orders of magnitude is found for the low-temperature region (below 543 K). For this region, the activation energy of the D.C. conduction mechanism process was evaluated using the Arrhenius relation $\sigma_{DC}T = \sigma_0 \exp(-E/kT)$. The estimated activation energy values were similar for ceramics doped with the same content of Fe and are listed in Figure 9. For the higher temperatures, the activation energy was impossible to estimate as the slope of curves changes continuously.

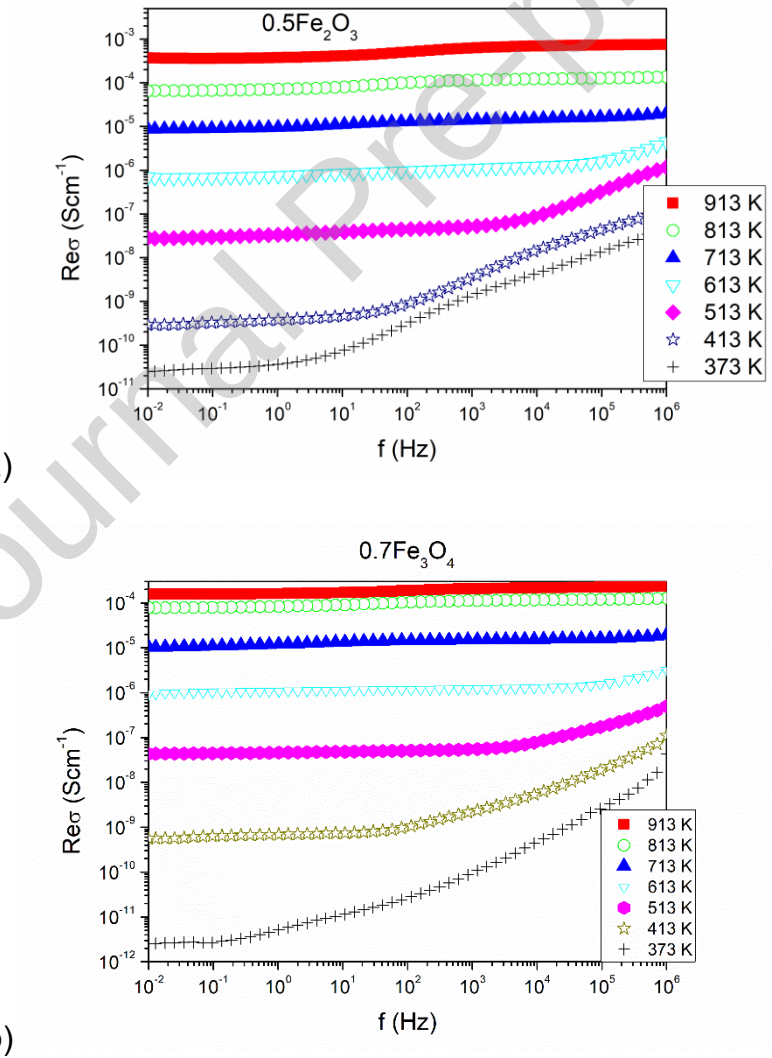

Figure 8. The real part of A.C. conductivity versus frequency for (a) $0.5Fe_2O_3$ and (b) $0.7Fe_3O_4$ samples showed for various temperatures.

Journal Pre-proof

MOST WIEDZY Downloaded from mostwiedzy.pl

The high-temperature D.C. conductivity of un-doped $Bi_4V_2O_{11}$ is about 10^{-4} Scm^{-1} at 913K [6]. The conduction mechanism is due to the hop of oxygen vacancies that occurred in ceramic. The formation of oxygen vacancies is the result of the occurrence of vanadium ions at reduced valance states V^{4+} and they are present in the perovskite-like layers of $(VO_{3.5}\square_{0.5})^{2-}$ [3]. The x= 0.5 substitution of V by Fe causes a slight increase in D.C. conductivity. The substitution of higher content of x = 0.7 vanadium ions results in a slight decrease in D.C. conductivity. The changes are the highest for the $0.7Fe_2O_3$ sample. In all Fe-containing ceramics, the unit cell of dominating $Bi_4V_{1.5}Fe_{0.5}O_{10.5}$ γ-phase is tetragonal while $Bi_4V_2O_{11}$ also exhibits tetragonal symmetry at high temperatures. However, in ceramics doped with 0.7 Fe, the small content of the orthorhombic $Bi_4Fe_{0.1}V_{1.9}O_{10.9}$ phase was also observed. This phase should also transform into tetragonal symmetry in the high-temperature region. Therefore, the observed small differences between conductivity in ceramics doped with different Fe contents can be due to the different concentration of oxygen vacancies, their disorder, and mobility which are determined during the synthesis. The increase in D.C. conductivity visible for x = 0.5 Fe might be due to the increase in the content of oxygen vacancies due to the ionic compensation of Fe-related acceptors. However, for higher doping levels the defect chemistry may be different. The increase in vacancies concentration became saturated and with further increase in dopant content, the charge compensation is different. For higher Fe amount the electronic p-type conductivity may start to be predominant whereas the oxygen ionic conductivity may play a minor role [31]. However, the observed D.C. conductivity decreases which mean that not only the defect chemistry but also the microstructure affects the total conductivity level. Probably for such a high Fe content the Fe_2O_3 nanocrystals may also affect the conductivity at high temperatures [32]. Iron oxide is a p-type electronic conductor with poor oxygen ionic conductivity. Thus the presence of this phase may increase the potential barrier for oxygen

Journal Pre-proof

MOST WIEDZY Downloaded from mostwiedzy.pl

ions hopping between the grains and in consequence the conductivity decreases.

At the middle-temperature range (between 543 and 763 K) the conduction mechanism is still due to oxygen vacancies in all materials. All Fe-containing ceramics exhibit higher D.C. conductivity than the un-doped one. It can be due to the different symmetry of unit cells. The $Bi_4V_2O_{11}$ exhibits orthorhombic symmetry (with lower conductivity) and the $Bi_4V_{1.5}Fe_{0.5}O_{10.5}$ has still tetragonal symmetry at this temperature range.

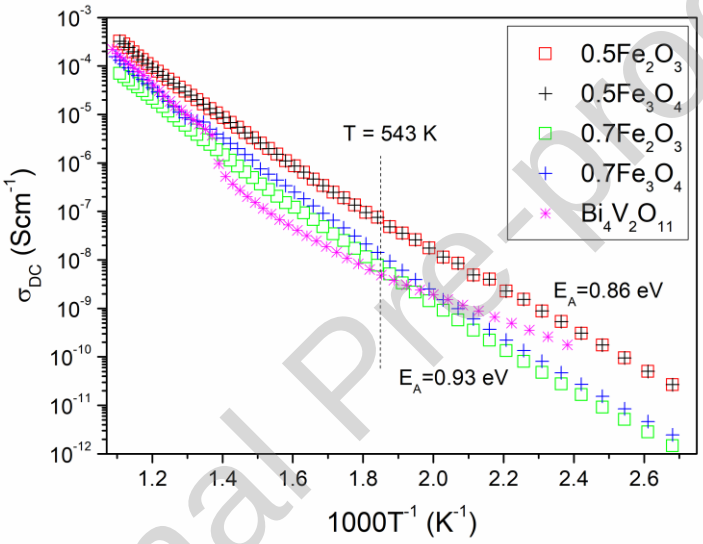

Figure 9. The D.C. conductivity versus reciprocal temperature for all samples. Additionally, the D.C. conductivity values for un-doped $Bi_4V_2O_{11}$ are added, taken from [2].

The low-temperature D.C. conductivity (below 543 K) of un-doped $Bi_4V_2O_{11}$ is about 10^{-10} Scm^{-1} (at 420 K) with an activation energy of 0.57 eV. The conduction mechanism can be still due to the hop of oxygen vacancies that occurred in ceramic. However the vanadium ions in the $Bi_4V_2O_{11}$ are present at two different valence states V^{4+} and V^{5+}, therefore there is also a possibility of a second electronic conduction mechanism [6,10,22,30,33]. The electronic conductivity is due to the reduction from V^{5+} to V^{4+} and the oxygen loss from the lattice. In perovskite-type oxides, the electron hopping between vanadium ions is usually described as the electron holes hopping from V^{5+} into V^{4+}.

Journal Pre-proof

MOST WIEDZY Downloaded from mostwiedzy.pl

Therefore, the conduction mechanism in the $Bi_4V_2O_{11}$ is mixed electronic-ionic which may explain the quite low activation energy [10,22]. The x = 0.5 substitution of V by Fe causes the increase in D.C. conductivity and activation energy up to 0.86 eV for x = 0.5 Fe. The substitution of higher content of x = 0.7 vanadium ions results in a slight decrease in D.C. conductivity and a further increase in activation energy up to 0.93 eV. With the substitution of vanadium ions by iron ions, the amount of vanadium ions is reduced. Consequently, the distance between the vanadium ions increases, as estimated from XRD results (see Tab. 2). These factors may increase the activation energy. Moreover, the crystalline Fe_2O_3 is also an electronic conductor with quite a high activation energy of 1.5 eV [32]. Its contribution is also visible as a decrease in the activation energy, especially in samples x = 0.7 Fe. It should be mentioned that the iron ions incorporated into the stoichiometry of grains are present only at Fe^{3+} coordination and do not take part in the conduction process.

4. Conclusions

The presence of the nanocrystals of Fe_2O_3 is the new observation made for $Bi_4V_{1.5}Fe_{0.5}O_{10.5}$ ceramic which was till now considered as single-phase material. Doping with the x = 0.7 Fe content caused the occurrence of the second orthorhombic $Bi_4Fe_{0.1}V_{1.9}O_{10.9}$ (Cmcm) phase. Moreover, the dominating tetragonal $Bi_4V_{1.5}Fe_{0.5}O_{10.5}$ (I4/mmm) phase was described by two different sets of lattice constants. The higher content of Fe dopant and using Fe_3O_4 instead of Fe_2O_3, assist in the nucleation of iron oxides nanocrystals on grains.

The substitution of x = 0.5 of Fe for V was enough to destroy the ferroelectric properties of $Bi_4V_2O_{11}$ ceramic. As the crystal structure was found to be tetragonal at room temperature, no phase transition around 730 K was observed. However, the small repetitive endothermic effect occurs at 916 K in both samples doped with = 0.5 Fe which is due to an order-disorder type γ ↔ γ′ phase transition. The small magnetic anomaly

Journal Pre-proof

MOST WIEDZY Downloaded from mostwiedzy.pl

correlated with Morin transition of hematite was detected in samples doped with x = 0.7 Fe. The conductivity behavior studied for all samples showed higher values for x = 0.5 Fe ceramics than for x = 0.7 Fe ones. The D.C. conduction process is dominated by the hop of oxygen vacancies in the wide temperature range. However, different defect chemistry for doping with Fe_3O_4 instead of Fe_2O_3 and the occurrence of Fe_2O_3 nanocrystals in x = 0.7 Fe samples caused the decrease in conductivity. At the low-temperature region, electron holes hopping is observed in all samples.

Acknowledgments

We want to thank Tadeusz Miruszewski for helping with the discussion about the conductivity process and Jacek Ryl for XPS measurements.

Data availability

The raw/processed data required to reproduce these findings cannot be shared at this time as the data also forms part of an ongoing study.

References

[1] O. Thery, R.N. Vannier, C. Dion, F. Abraham, Preparation, characterization and oxide ion conductivity in U-substituted Bi4V2O11, Solid State Ionics. 90 (1996) 105–110. https://doi.org/10.1016/s0167-2738(96)00359-1.

[2] O. Joubert, M. Ganne, R.N. Vannier, G. Mairesse, Solid phase synthesis and characterization of new BIMEVOX series: $Bi_4V_{2-x}M_xO_{11-x}$ (M = CrIII, FeIII), Solid State Ionics. 83 (1996) 199–207. https://doi.org/10.1016/0167-2738(96)00009-4.

[3] R.N. Vannier, E. Pernot, M. Anne, O. Isnard, G. Nowogrocki, G. Mairesse, $Bi_4V_2O_{11}$ polymorph crystal structures related to their electrical properties, Solid State Ionics. 157 (2003) 147–153. https://doi.org/10.1016/S0167-2738(02)00202-3.

[4] G. Mairesse, P. Roussel, R.N. Vannier, M. Anne, G. Nowogrocki, Crystal structure

MOST WIEDZY Downloaded from mostwiedzy.pl

determination of α-, β- and γ-$Bi_4V_2O_{11}$ polymorphs. Part II: Crystal structure of α-Bi4V2O11, Solid State Sci. 5 (2003) 861–869. https://doi.org/10.1016/S1293-2558(03)00016-5.

[5] R.N. Vannier, G. Mairesse, F. Abraham, G. Nowogrocki, W-substituted $Bi_4V_2O_{11}$, Solid State Ionics 80 (1995) 11–17. **DOI:** 10.1016/0167-2738(95)00123-N**.**

[6] N. A. Szreder, P. Kupracz, M. Prześniak-Welenc, J. Karczewski, M. Gazda, R.J. Barczyński, Nonlinear and linear impedance of bismuth vanadate ceramics and its relation to structural properties, Solid State Ionics. 271 (2015) 86–90. https://doi.org/10.1016/j.ssi.2014.10.028.

[7] R. Kant, K. Singh, O.P. Pandey, Synthesis and characterization of bismuth vanadate electrolyte material with aluminum doping for SOFC application, Int. J. Hydrogen Energy. 33 (2008) 455–462. https://doi.org/10.1016/j.ijhydene.2007.07.025.

[8] M. Guillodo, J. Fouletier, L. Dessemond, P. Del Gallo, Electrical properties of dense Me-doped bismuth vanadate (Me= Cu, Co) pO2-dependent conductivity determined by impedance spectroscopy, J. Eur. Ceram. Soc. 21 (2001) 2331–2344. https://doi.org/10.1016/S0955-2219(01)00214-X.

[9] K. Sooryanarayana, T.N. Guru Row, K.B.R. Varma, Crystal structure of ferroelectric $Bi_2VO_{5.5}$, Mater. Res. Bull. 32 (1997) 1651–1656. https://doi.org/10.1016/S0025-5408(97)00157-8.

[10] N.A. Szreder, P. Kupracz, M. Prześniak-Welenc, J. Karczewski, M. Gazda, K. Siuzdak, R.J. Barczyński, Electronic and ionic relaxations in strontium-borate glass and glass-ceramics containing bismuth and vanadium oxides, Solid State Ionics. 282 (2015). https://doi.org/10.1016/j.ssi.2015.09.021.

[11] K. Shantha, K.B.R. Varma, Preparation and characterization of nanocrystalline

Journal Pre-proof

MOST WIEDZY Downloaded from mostwiedzy.pl

powders of bismuth vanadate, Mater. Sci. Eng. B Solid-State Mater. Adv. Technol. 60 (1999) 66–75. https://doi.org/10.1016/S0921-5107(99)00021-5.

[12] K. Shantha, K.B.R. Varma, Frequency dependence of the dielectric properties of ferroelectric $Bi_2VO_{5.5}$ ceramics, Solid State Ionics. 99 (1997) 225–231.

[13] N.A. Wójcik, P. Kupracz, R.J. Barczyński, B. Jonson, S. Ali, Ion conduction in beryllium-alumino-silicate glasses doped with sodium or sodium and lithium ions, Solid State Ionics. 341 (2019) 115055. https://doi.org/10.1016/j.ssi.2019.115055.

[14] N.A. Wójcik, B. Jonson, R.J. Barczyński, P. Kupracz, D. Möncke, S. Ali, Electrical properties of Na_2O-CaO-P_2O_5 glasses doped with SiO_2 and Si_3N_4, Solid State Ionics. 325 (2018) 157–162. https://doi.org/10.1016/j.ssi.2018.08.011.

[15] E.D. Politova, E.A. Fortalnova, G.M. Kaleva, A. V. Mosunov, M.G. Safronenko, N.U. Venskovskii, Solid solutions on the base of bismuth vanadate: Preparation, structure, phase transitions, dielectric and transport properties, Solid State Ionics. 192 (2011) 248–251. https://doi.org/10.1016/j.ssi.2010.06.047.

[16] S. Beg, N.A.S. Al-Areqi, S. Haneef, Study of phase transition and ionic conductivity changes of Cd-substituted $Bi_4V_2O_{11-\delta}$, Solid State Ionics. 179 (2008) 2260–2264. https://doi.org/10.1016/j.ssi.2008.08.008.

[17] S. Beg, N.S. Salami, Study on the electrical properties of Co-Ti double substituted $Bi_4V_2O_{11}$, J. Alloys Compd. 586 (2014) 302–307. https://doi.org/10.1016/j.jallcom.2013.10.061.

[18] M. Alga, A. Ammar, R. Essalim, B. Tanouti, F. Mauvy, R. Decourt, Synthesis, sintering and electrical properties of P-doped $Bi_4V_2O_{11}$ ceramics, Solid State Sci. 7 (2005) 1173–1179. https://doi.org/10.1016/j.solidstatesciences.2005.06.011.

[19] R.J. Barczyński, N. A. Szreder, J. Karczewski, M. Gazda, Electronic conductivity in

Journal Pre-proof

MOST WIEDZY Downloaded from mostwiedzy.pl

the SiO_2–PbO–Fe_2O_3 glass containing magnetic nanostructures, Solid State Ionics. 262 (2013) 5–9. https://doi.org/10.1016/j.ssi.2013.10.008.

[20] A. Lenarciak, N.A. Wójcik, P. Kupracz, J. Strychalska-Nowak, Z. Sobczak, M. Prześniak-Welenc, J. Karczewski, R.J. Barczyński, Thermal, electrical, and magnetic properties of Fe_2O_3–PbO–SiO_2 glass prepared by traditional melt-quenching and twin roller fast-cooling methods, J. Phys. Chem. Solids. 135 (2019). https://doi.org/10.1016/j.jpcs.2019.05.007.

[21] N.A. Wójcik, N.S. Tagiara, S. Ali, K. Górnicka, H. Segawa, T. Klimczuk, B. Jonson, D. Möncke, E.I. Kamitsos, Structure and magnetic properties of BeO-Fe_2O_3-Al_2O_3-TeO_2 glass-ceramic composites, J. Eur. Ceram. Soc. 41 (2021) 5214–5222. https://doi.org/10.1016/j.jeurceramsoc.2021.04.005.

[22] N.A. Wójcik, M. Prześniak-Welenc, P. Kupracz, J. Karczewski, M. Gazda, R.J. Barczyński, Mixed ionic–electronic conductivity and structural properties of strontium-borate glass containing nanocrystallites of $Bi_2VO_{5.5}$, Phys. Status Solidi B 254 (2017). https://doi.org/10.1002/pssb.201700093.

[23] N.A. Wójcik, N.S. Tagiara, D. Möncke, E.I. Kamitsos, S. Ali, J. Ryl, R.J. Barczyński, Mechanism of hopping conduction in Be–Fe–Al–Te–O semiconducting glasses and glass–ceramics, J. Mater. Sci. 57 (2022) 1633–1647. https://doi.org/10.1007/s10853-021-06834-w.

[24] A.A. Krylov, Y. V. Emelyanova, E.S. Buyanova, M. V. Morozova, A.I. Vylkov, A.Y. Chuykin, Materials based on BIFEVOX and bismuth or iron simple oxides nanopowders, Chim. Techno Acta. 4 (2017) 202–208. https://doi.org/10.15826/chimtech/2017.4.3.05.

[25] G. Paściak, J. Chmielowiec, P. Bujłło, New ceramic superionic materials for IT-SOFC applications, Mater. Sci. Pol. 23 (2005) 209–219.

Journal Pre-proof

MOST WIEDZY Downloaded from mostwiedzy.pl

[26] J. Sunarso, S. Baumann, J.M. Serra, W.A. Meulenberg, S. Liu, Y.S. Lin, J.C. Diniz da Costa, Mixed ionic-electronic conducting (MIEC) ceramic-based membranes for oxygen separation, J. Memb. Sci. 320 (2008) 13–41. https://doi.org/10.1016/j.memsci.2008.03.074.

[27] P. Fuierer, M. Maier, J. Exner, R. Moos, Anisotropy and thermal stability of hot-forged BICUTIVOX oxygen ion conducting ceramics, J. Eur. Ceram. Soc. 34 (2014) 943–951. https://doi.org/10.1016/j.jeurceramsoc.2013.10.016.

[28] F.J. Morin, Magnetic Susceptibility of α-Fe_2O_3 and α-Fe_2O_3 with Added Titanium, Phys. Rev. 78 (1950) 819–820. https://doi.org/10.1103/PhysRev.78.819.2.

[29] A. Popelka, S. Zavahir, S. Habib, Chapter 2 - Morphology analysis, in: Polymer Science and Innovative Applications, Elsevier, 2020: pp. 21–68. https://doi.org/10.1016/B978-0-12-816808-0.00002-0.

[30] N.A. Wójcik, P. Kupracz, R.J. Barczyński, Nonlinear electrical properties of glass-ceramics nanocomposites containing ferroelectric nanocrystallites of $Bi_2VO_{5.5}$, Solid State Ionics. 317 (2018) 7–14. https://doi.org/https://doi.org/10.1016/j.ssi.2017.12.035.

[31] T. Miruszewski, W. Skubida, A. Dawczak, K. Dzierzgowski, S. Wachowski, A. Mielewczyk-Gryń, M. Gazda, Structure and transport properties of donor-doped barium strontium cobaltites, J. Eur. Ceram. Soc. 41 (2021) 7098–7104. https://doi.org/10.1016/j.jeurceramsoc.2021.07.018.

[32] B.M. Warnes, F.F. Aplan, G. Simkovich, Electrical conductivity and seebeck voltage of Fe_2O_3, pure and doped, as a function of temperature and oxygen pressure, Solid State Ionics 12 (1984) 271–276. https://doi.org/10.1016/0167-2738(84)90156-5.

[33] M. Prześniak-Welenc, N. A. Szreder, a. Winiarski, M. Łapiński, B. Kościelska, R.J.

Journal Pre-proof

MOST WIEDZY Downloaded from mostwiedzy.pl

Barczyński, M. Gazda, W. Sadowski, Electrical conductivity and relaxation processes in V_2O_5 nanorods prepared by sol-gel method, Phys. Status Solidi. 6 (2015). https://doi.org/10.1002/pssb.201552113.

Declaration of competing interest

☒ The authors declare that they have no known competing financial interests or personal relationships that could have appeared to influence the work reported in this paper.

☐The authors declare the following financial interests/personal relationships which may be considered as potential competing interests:

The summary of novel conclusions:

- High-conducting $Bi_4V_{2-x}Fe_xO_{11-\delta}$ ceramics containing Fe_2O_3 nanocrystals were synthesized.
- Doping with higher Fe content and using Fe_3O_4 reagent instead of Fe_2O_3 supported the nucleation of iron oxides nanocrystals.
- The presence of Fe_2O_3 nanocrystals was noticed in magnetic properties as Morin transition characteristic for hematite.
- The order-disorder type γ ↔ γ´ phase transition was found at 916 K in samples doped with x = 0.5 Fe.
- The conductivity was improved through substitution of V by 0.5 Fe while for higher substitution it was improved only at the middle-temperature range.

Journal Pre-proof

MOST WIEDZY Downloaded from mostwiedzy.pl